Performance of IceTop as a veto for IceCube

The IceCube Collaboration[†]

[†] *http://icecube.wisc.edu/collaboration/authors/icrc17_icecube*

E-mail: `delia.tosi@icecube.wisc.edu`

The IceCube Neutrino Observatory features a kilometer-cubed deep detector and a surface component, IceTop. IceTop consists of 162 ice-filled tanks equipped with optical sensors capable of detecting charged particles produced in air showers. While IceTop is well known for its cosmic-ray spectrum and mass composition measurements, it can also be used as a veto for IceCube. This role is becoming more important in the design of a larger surface array. High-energy neutrinos are absorbed by the Earth, therefore detecting neutrinos from the southern hemisphere is a priority. An efficient veto, however, requires suppressing the large background consisting of penetrating atmospheric muons and neutrinos. A surface array like IceTop can reduce the background by identifying particles which are generated in the same air shower as the muons in the deep detector. The capabilities and limitations of IceTop as a veto for cosmic rays will be presented.

Corresponding authors: Delia Tosi[1], Hershal Pandya[*2]

[1]*Dept. of Physics and Wisconsin IceCube Particle Astrophysics Center, University of Wisconsin, Madison, WI 53706, USA*

[2]*Dept. of Physics and Astronomy, University of Delaware, Newark, DE 19711, USA*

---

[*]Speaker.

1. Introduction

The IceCube Neutrino Observatory is a particle detector located at the geographic South Pole [1]. The experiment features two components. The in-ice neutrino telescope (IceCube) consists of 86 strings each equipped with 60 digital optical modules (DOMs), installed at depths between 1450 m and 2450 m. The surface component (IceTop) includes 81 stations, each with two tanks 10 m apart located in proximity of the top of each in-ice string. Each tank contains frozen water and is equipped with two DOMs. The DOMs of both arrays feature photomultiplier tubes (PMT) able to detect, at single photon level, the Cherenkov radiation emitted by secondary charged particles. On the surface, these are charged leptons produced in hadronic or electromagnetic interactions in the atmosphere. In ice, these are either penetrating muons from showers, or particles produced by neutrino interactions in the Antarctic ice cap or in the bedrock.

The goal of the analysis presented in this paper is to study the veto capabilities of IceTop using air showers that are too low in energy to trigger the array, but which are coincident with muon events in IceCube. While the veto possibilities of IceTop were included in the original design of the array, a thorough study of its efficiency as a veto over a wide energy range is still underway.

Currently, the highest purity sample of astrophysical neutrinos is obtained isolating neutrino interactions starting in the instrumented volume of IceCube. In this sample, muon tracks are particularly important given their superior angular reconstruction, necessary for real time alerts and multi-messenger searches [2]. The immense majority of down-going muons entering IceCube are penetrating atmospheric muons or atmospheric neutrino–induced muons, and they constitute the main background in the search for astrophysical neutrinos. However, above a few hundred TeV muon energy, a muon track starting in the detector has a higher chance to be produced by the charged-current interaction of an astrophysical muon neutrino than by an atmospheric interaction, due to the harder spectral index of astrophysical neutrinos. The high energy starting track analysis [3] is highly effective in selecting astrophysical neutrinos, but it relies on using the outer shell of the IceCube detector as a veto, greatly decreasing the effective volume. A surface detector capable of identifying cosmic ray showers producing such tracks can effectively increase the detector volume of IceCube up to the surface, and extend the field of view towards the center of the Galaxy [4].

2. Method

2.1 Data Selection

The method presented here uses selection cuts substantially identical to those in the analysis presented in [5]. An offline filter selects events which have more than 1000 photoelectrons (PE) deposited in IceCube: this has a rate between 1 Hz and 2 Hz. Of these events we keep those which also have an *homogenized charge* $Q_{toth} > 1000$ PE, defined as the total charge calculated after removing those DOMs which have detected more than 50% of the total charge deposited. This last cut removes the so called *balloon events*, i.e. events where one DOM reports a disproportionate charge due to a muon track passing very close. We also require that the event is reconstructed as down-going, and that the muon track length in the detector is L>800 m. Finally, the muon track trajectory extrapolated to surface needs to intersect the IceTop footprint at a *impact point* located inside the detector and at a distance S>62.5 m from the perimeter of IceTop (see Fig. 1).

These cuts remove all the tracks with reconstructed zenith angle $\theta > 32°$ and reduce the number of events drastically to 1.8 % of the event selection we start with. The numeric values for L and S have not been yet optimized for this analysis.

The vast majority of the in-ice triggers selected with the above method are associated with cosmic ray showers. At sufficiently high energy these have clear signatures in IceTop: multiple DOMs detect photoelectrons (*hits*) induced by shower particles, allowing for the reconstruction of its energy and direction. As our focus is to link muon tracks with showers which have not necessarily triggered IceTop, we do not require an IceTop trigger and we use only information about the muon track obtained from the in-ice detector.

The muon direction is determined by a likelihood-based algorithm which fits the first arrival times and charge on all the DOMs in the detector, assuming an analytical parametrization of the Cherenkov light intensity as a function of distance to the muon track [7].

Figure 1: Illustration of the cuts used to select events for this analysis: L>800 m and S>62.5 m.

This reconstructed direction is then used as seed for a second fitting algorithm, which fits for the time of the interaction using only the time of the first unscattered photon and the total charge in each DOM. The combination of these steps provides better agreement between true and reconstructed values in simulation.

A proxy for the muon energy, called MuEx, is determined by fitting the expected number of photons via an analytic template which scales with the energy of the muon [6]. This energy estimator accounts for energy losses outside the detector and it is therefore more accurate than a simple sum of the DOM charges. A calibration of the energy proxy to the muon or muon bundle energy requires a high statistics simulation, not necessary for the goal of this analysis, therefore the values of MuEx are given in the following in arbitrary units.

The MuEx and zenith distribution of events remaining after the selection is shown in Fig. 6a and Fig. 6b for 10% of the data collected in 2012. The rise in event numbers up to $\log_{10}(\text{MuEx}) \sim 4$ is a threshold effect due to the use of $Q_{toth} > 1000$ PE for the event selection.

2.2 Signal simulation

Event rates for astrophysical neutrinos are estimated using NEUTRINOGENERATOR, a Monte Carlo simulation program based on ANIS [8]. Neutrinos are generated and propagated through the Earth using CTEQ cross section tables [9], and are forced to interact before passing through the detector volume; the true interaction probability is assigned to each neutrino interaction as a weight. For this analysis a general purpose dataset of muon neutrinos with a spectrum proportional to E^{-1} over an angular range of $0° \leq \theta \leq 180°$ and energy range of 10^2 GeV $\leq E_\nu \leq 10^7$ GeV was used. The same data selection criteria as explained in section 2.1 was applied. To obtain the signal

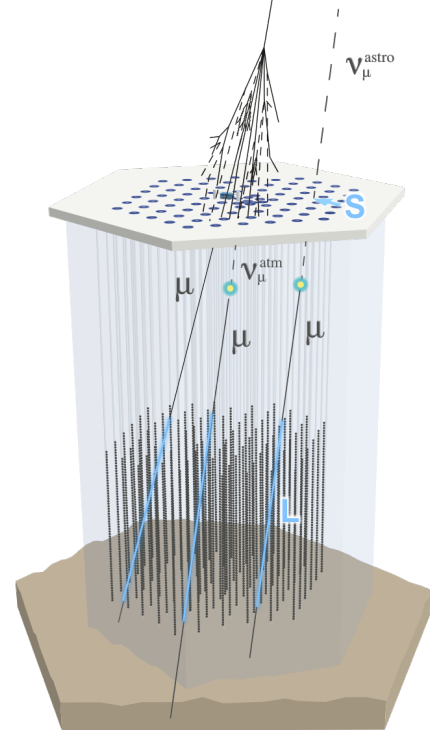spectrum the surviving events were re-weighted to the best fit astrophysical neutrino spectrum of $\phi_{\nu+\bar{\nu}} = \left(0.90^{+0.30}_{-0.27}\right) \times 10^{-18} \text{GeV}^{-1}\text{cm}^{-2}\text{s}^{-1}\text{sr}^{-1} \cdot (\text{E}_\nu/100\,\text{TeV})^\gamma$ with $\gamma = -2.13 \pm 0.13$ [10]. The calculated expected number of events for astrophysical neutrinos and cosmic rays is shown in Fig. 6. At $\log_{10}\text{MuEx} \sim 5$, a factor on the order of $\sim 10^5$ is required to reduce the background from cosmic rays to the level of astrophysical neutrinos.

The current simulation produced with NEUTRINOGENERATOR does not include IceTop hits, therefore with simulation it is not possible to develop cuts based on the temporal and spatial correlation of IceTop hits with in-ice muon tracks. To overcome this issue we process every recorded event of a certain time length in the final selection in the following way: we replace all the IceTop hits with a same duration snapshot of IceTop hits extracted from a fixed rate trigger recorded within hours from each recorded event. The fixed rate trigger is a 10 ms unbiased recording of the whole detector taken at a fixed rate (every 30 seconds). Given the long duration of the recording, fixed rate triggers contain a number of other naturally occurring triggers. For this analysis we do not use any fixed rate triggers which have also satisfied an IceTop trigger. The dataset obtained with this method resembles neutrino-like signals, and includes all the systematics of the detector, such as the temporal variation of IceTop DOMs hit rates (due to temperature and snow depth) and cross correlation of hits between DOMs in a single tank due to stray muons, and DOM inherent features like after-pulsing and pre-pulsing [11]. This sample is referred to in the following as the *randomized sample* or neutrino-like (ν-like) sample and is compared with the experimental cosmic ray data (cr-data) sample.

2.3 Data Processing

Given an event in IceCube, the muon track direction is assumed to represent the axis of the cosmic ray shower producing the muon. For each tank we calculate the perpendicular *lateral distance* from the shower axis and the expected arrival time of the shower at the tank, after extrapolating the muon track to the surface and using a data-derived model for the curvature of the shower front. If a tank did not record a hit or was not operational at the time of the event, we record its distance and we keep track of the tank status. If a tank has a hit, we record the *residual time t_{res}*, defined as the difference between the recorded and the expected time. In order to keep the normalization correct it is necessary to

Figure 2: Template used to select one hit per tank per event, showing the distribution of all the hits residual times (see text) for all the events in the selection. The inset shows a zoomed-in version.

require at most one pulse per tank per event, so that the sum of tanks with or without hits and the tanks not operational at the event time is constant in all the events considered.
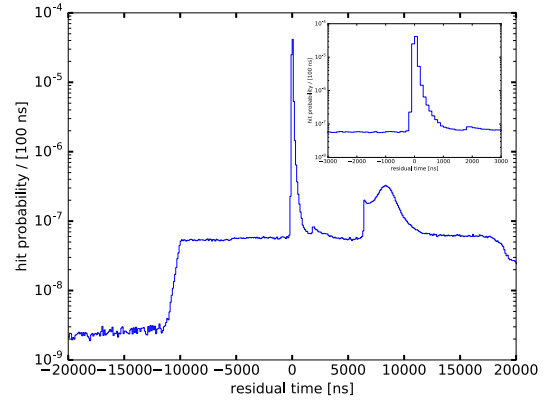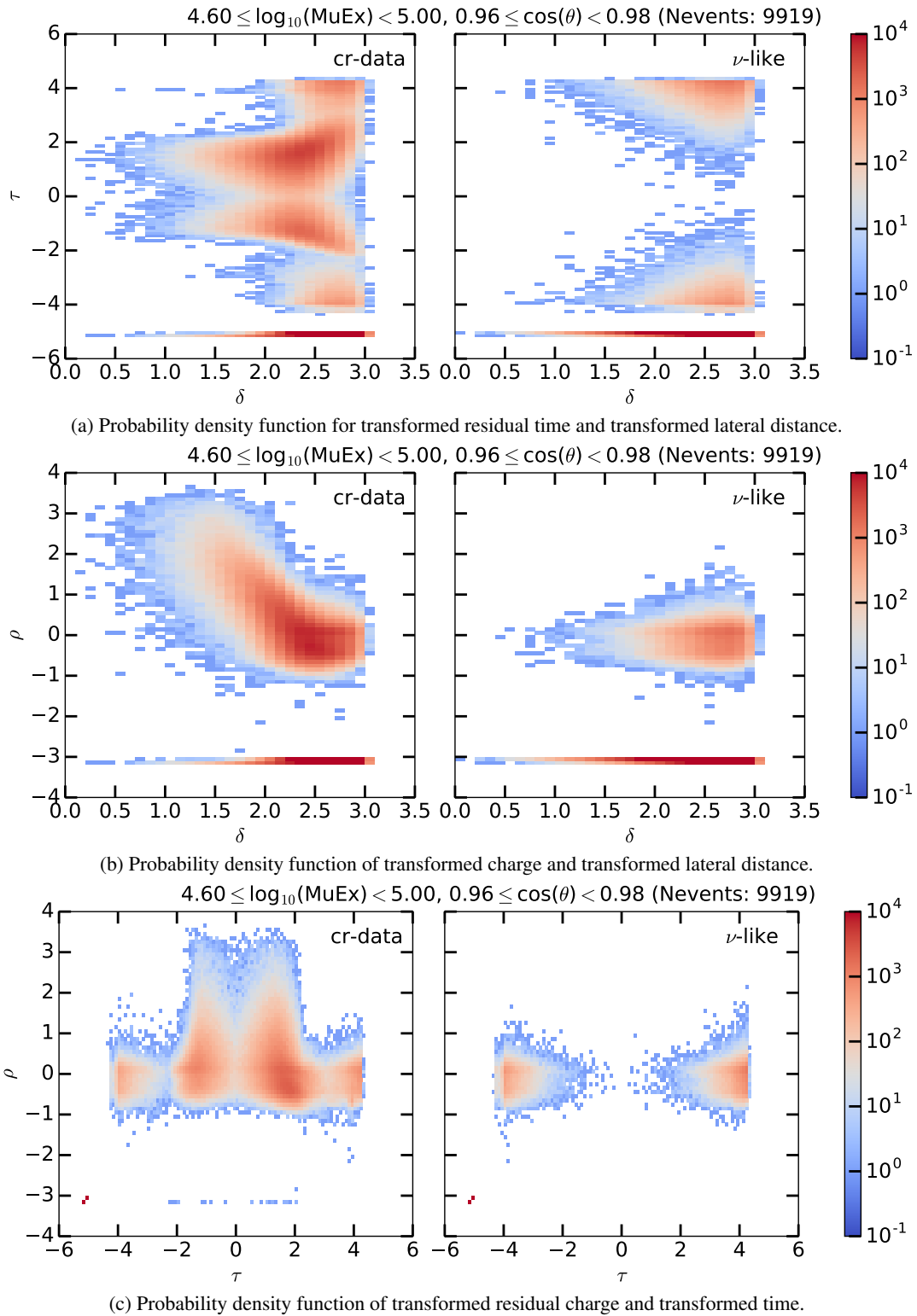
(a) Probability density function for transformed residual time and transformed lateral distance.

(b) Probability density function of transformed charge and transformed lateral distance.

(c) Probability density function of transformed residual charge and transformed time.

Figure 3: 2D-PDFs for one energy, zenith bin. The variables shown are residual time, lateral distance and charge detected by IceTop DOMs with the transformation of coordinates as explained in the text. The left column shows the experimental data, the right column shows the randomized sample. The bands at the bottom represent non-operational DOMs or DOMs which did not record a hit.

If the two DOMs in a tank have more than one hit, we remove all hits but the one which has the highest probability to be correlated with the cosmic ray shower. This probability is calculated from a one-dimensional probability density function derived from the residual times of all the hits. The data-derived template is shown in Fig. 2. The central spike corresponds to the shower front, while the bumps at later times are due to a combination of ADC's dead time and PMT after-pulses [1, 11].

For each hit surviving the selection, we also track the charge Q_i recorded by the DOM in tank i, which is expressed in units of *Vertical Equivalent Muon* (VEM) [12].

To increase the weight of hits near in time or space to the shower front, we use a logarithmic binning. Since residual times can be negative and have values between 0 and 1 ns, we apply a coordinate transformation and define $\tau = $ sign $(t_{res}) \cdot \log_{10}(|t_{res}|+1)$. We use a similar coordinate transformation for the lateral distance (always positive by definition) since it can also have values ≤ 1 m. We call the new parameters *transformed residual time τ* and *transformed lateral distance δ*. As for the charge, we define the parameter *transformed charge $\rho = \log_{10}(Q)$*.

2.4 PDFs and LLH Ratio

Using the observables defined above $(\rho_i, \tau_i, \delta_i)$ we construct three two-dimensional PDFs as shown in Fig. 3 for one example energy and zenith bin for the experimental dataset (representing the cr-data sample) on the left and the randomized sample (representing the ν-like sample) on the right. From the comparison between each PDF for the two datasets, the cosmic rays signature is visible as a larger number of hits near the shower front and in the higher charge distribution (i.e. at small values of τ and δ and large values of ρ). The larger population of hits at large values of δ is due to geometry (a larger number of tanks is available at larger radius). The randomized sample shows the distribution of hits in the same variables for neutrino-like events. Sections of each PDF are shown in the corresponding linear variables in Fig. 4. For a given event, a log-likelihood (LLH) ratio is constructed using three sets of PDFs. For example, the LLH ratio (LLHR) using the τ_i vs.
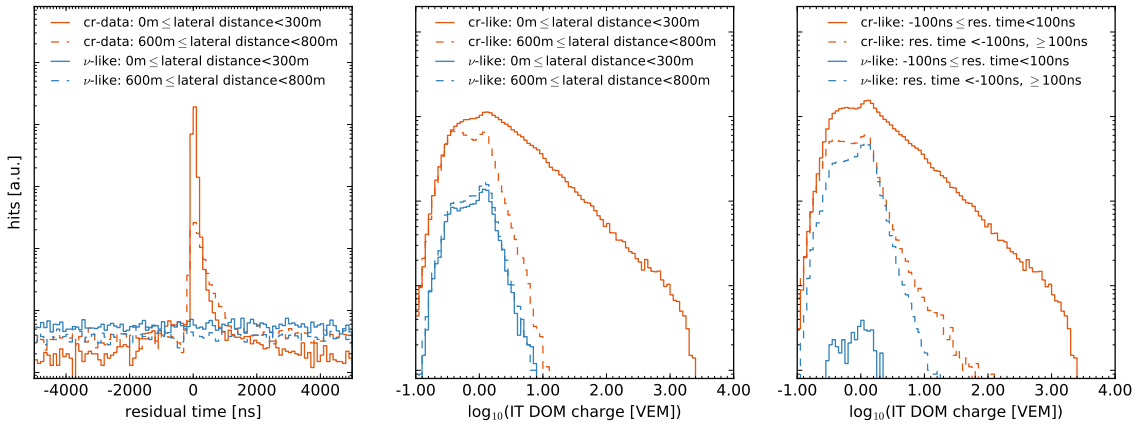

Figure 4: Each plot shows the equivalent of a slice for each two-dimensional PDF as shown in Fig. 3, for cr-data and ν-like samples and for two selected ranges of lateral distance or residual times, close or far from the shower front. The cr-data sample shows more hits and larger charge near the shower front than the ν-like sample.

δ_i PDF is constructed as follows:

$$\text{LLH Ratio} = \log_{10}\left(\frac{L(\{(\tau_i,\ \delta_i)\}\,|H_{CR})}{L(\{(\tau_i,\ \delta_i)\}\,|H_\nu)}\right) \tag{2.1}$$

where the individual log-likelihoods are defined as

$$L(\{(\tau_i,\ \delta_i)\}\,|H) = \prod_{i=1}^{N_{Tanks}} P(\tau_i,\ \delta_i|H) \tag{2.2}$$

Here $P(\tau_i,\ \delta_i|H)$ is the probability of having a tank with transformed residual time τ_i and transformed lateral distance δ_i in the PDF constructed using hypothesis H (H = CR or ν). The LLHR distribution is shown for each template and for one example energy and zenith bin in Fig. 5.

Given each LLHR distribution we calculate the LLHR cut value that retains a predefined fraction (for example 100% and 90%) of the randomized sample events in the distribution. The three distributions are treated as independent, so the fraction of neutrinos retained as

Figure 5: Log-likelihood ratio for one energy and zenith bin, for the three two dimensional PDFs shown in Fig. 3.

a result is 100% in the first case. In the second case, the fraction of neutrinos retained depends on energy and zenith bin; overall 80% neutrinos are retained. We then count how many cosmic rays pass such cuts as a function of zenith angle and muon energy proxy. We then rescale the number of passing events taking into account that the sample analyzed corresponds to ∼1/11 of the livetime of the 2012 dataset. The effect of such cuts on the distribution of events at the final selection is shown as a function of the muon energy proxy (integrated over all the zenith angles) in Fig. 6a and as a function of the cosine of zenith angle (integrated over all the energies) in Fig. 6b. Where no events pass the LLHR cuts, we show the 68% confidence level upper limit.

3. Results

The preliminary veto efficiency, calculated with the log-likelihood method presented here, is shown vs energy and vs zenith in Fig. 7a-7b. With a 80% (100%) retaining fraction of astrophysical neutrinos, in the energy bin between $4.6\leq \log_{10}(\text{MuEx})<4.8$ $(4.8\leq \log_{10}(\text{MuEx})<5.0)$, none of the 7622 events in the sample passes the cuts. At this energy and above we show therefore the 68% upper limit. In the energy bin between $4.4\leq \log_{10}(\text{MuEx})<4.6$ $(4.6\leq \log_{10}(\text{MuEx})<4.8)$, 11 (6) events out of 48197(26803) pass the cuts, with the method achieving a background passing rate (equivalent to 1.0 − veto rejection efficiency) of 2.3×10^{-4} (2.2×10^{-4}). No events are found in the selection with $\log_{10}(\text{MuEx})\geq 6.2$.

A further optimization of the cuts is possible, and other methods to combine the three different log-likelihood discriminators are being investigated. More statistics will be added in order to improve the veto efficiency at high energy, where the current estimate is statistically limited. The method will be used to explore requirements for a future extended veto.
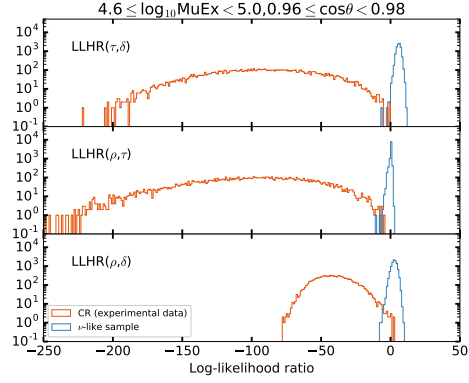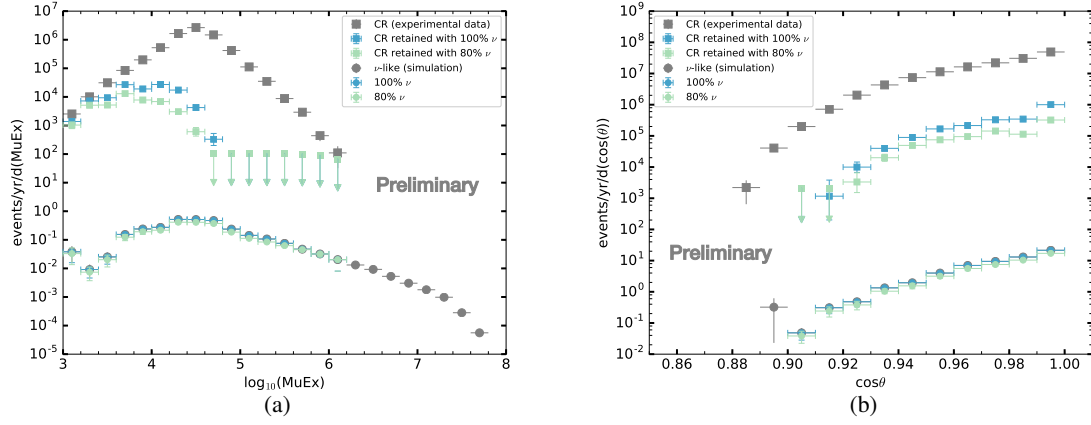
Figure 6: Event rates for background (data) and signal (calculated with simulation), versus in-ice muon energy proxy (a) and versus cosine of zenith angle (b) at the final selection level and after applying a cut which retains 100% and 80% neutrinos. The rise in event numbers up to $\log_{10}(\text{MuEx}){\sim}4$ is due to the selection of events being based on a different energy proxy (see section 2.1). Arrows indicate upper limits.
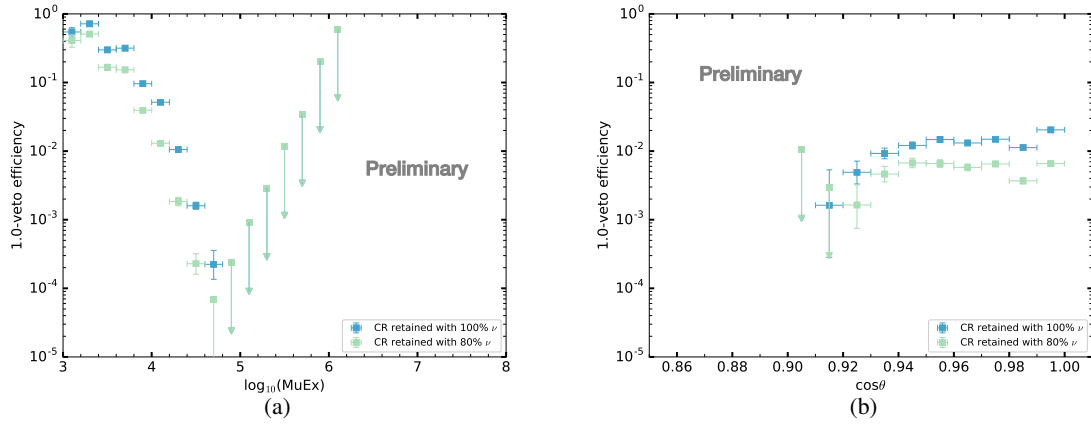

Figure 7: Veto efficiency calculated from analyzed sample, versus in-ice muon energy proxy (a) and versus cosine of zenith angle (b). The arrows denote upper limits.

References

[1] **IceCube** Coll., M. G. Aartsen et al., *J. Inst.* **12** P03012 (2017).

[2] **IceCube** Collaboration, `PoS(ICRC2015)022` (2015).

[3] **IceCube** Coll., `PoS(ICRC2017)981` (these proceedings).

[4] **IceCube** Collaboration, `PoS(ICRC2015)1156` (2015).

[5] **IceCube** Coll., `PoS(ICRC2015)1086` (2015).

[6] **IceCube** Coll., M. G. Aartsen et al., *J. Inst.* **9** P03009 (2014).

[7] **AMANDA** Coll., J. Ahrens et al., *Nucl. Instrum. Meth.* **A524** 169-194 (2004).

[8] A. Gazizov and M. P. Kowalski, *Comput. Phys. Commun.* **172** 203-213 (2005).

[9] R. Gandhi, C. Quigg, M. H. Reno, I. Sarcevic *Phys. Rev.* **D58** 093009 (1998).

[10] **IceCube** Coll., M. G. Aartsen et al., *Astrophys. J.* **833** 3 (2016).

[11] **IceCube** Coll., R. Abbasi et al., *Nucl. Instrum. Meth.* **A618** 139-152 (2010).

[12] **IceCube** Coll., R. Abbasi et al., *Nucl. Instrum. Meth.* **A700** 188 (2013).